Ultrasonic Nozzle Spray in Situ Mixing and Microwave-Assisted Preparation of Nanocrystalline Spinel Metal Oxides: Nickel Ferrite and Zinc Aluminate

Edward K. Nyutu,[†] William C. Conner,[§] Scott M. Auerbach,[||] Chun-Hu Chen,[†] and Steven L. Suib*[,†,‡]

Departments of Chemistry and of Chemical, Materials and Bimolecular Engineering, University of Connecticut, Storrs, Connecticut 06269, and Departments of Chemical Engineering and of Chemistry, University of Massachusetts, Amherst, Massachusetts 01003

Received: July 18, 2007; In Final Form: October 30, 2007

Nanocrystalline spinel nickel ferrite and zinc aluminate particles (6−20 nm) can be prepared by a recently developed continuous flow method that combines microwave heating and in situ ultrasonic nozzle spray mixing. The preparations were carried out at ambient pressure (1 atm), microwave power (0−600 W), and ultrasonic nozzle with resonant frequency of 48 or 120 kHz. The products were characterized by X-ray diffraction, field emission scanning electron microscopy, transmission electron microcopy, X-ray electron dispersive spectroscopy, Brunauer−Emmett−Teller spectroscopy, Raman spectroscopy, Fourier transform infrared spectroscopy, thermogravimetric analysis, and temperature-programmed desorption mass spectrometry. The results showed that the ultrasonic nozzle and microwave irradiation complement each other, with respect to the purity of the products. The specific advantages of INM method for the preparing nickel ferrites are that pure materials with high surface areas and tunable particle sizes are produced, and this process is continuous.

Introduction

Metal oxide nanoparticles are of great interest due to their practical applications as high-temperature ceramics, gas sensors, optical coatings, and magnetic, biomedical, and catalytic materials.[1] Fabrication of particles with controlled morphologies, particle sizes, compositions, and purity requires precise control of synthesis parameters.[1] Hence, processes and methods that control these parameters and lead to particles of certain characteristics are of crucial importance.

Spinel metal oxide particles are produced by techniques such as hydrothermal methods, coprecipitation, microemulsions, combustion, sol−gel, solvothermal, electrodeposition, sonochemical decomposition, nonaqueous routes, and also solid-state reactions.[1−2] The coprecipitation of oxides from aqueous solutions is widely used to prepare high purity nanoparticles of single or multicomponent oxides.[1] However, production of oxides by precipitation methods is not a straightforward process.[1a,1f] Synthesis of most spinels is carried out as a batch operation, though there are few reports of flow synthesis of nanoparticles in continuous segmented flow tubular microreactors[1c,f,j] and with hydrothermal flow injection.[3] Batch systems have certain limitations such as uncontrolled mixing and uniform residence time resulting in particles with a broad particle size distribution due to an inhomogeneous growth rate, secondary nucleation, and particle ripening.[1a,c,j,2j,4] A flow reactor can generate products on a continuous basis and is more desirable than batch reactors for large-scale production.

Microwave irradiation has been employed in many chemical reactions and has been found to be more effective in selective heating in many processes.[5] These processes are understood to be more environmentally friendly and require less energy than conventional methods.[5,6] The exact nature of microwave interactions with reactants and subsequent increased rate of chemical transformations is somewhat unclear and is extensively debated.[5,6] Nevertheless, the energy transfer from microwaves to the material is believed to occur either through resonance or relaxation, which results in rapid heating.

Ultrasonic nozzle spray processes involve the generation of fine, low velocity mist from an initial solution that contains dissolved precursors.[6−8] In the case of coprecipitation reactions, the pH and method of mixing of the precursor solutions significantly affect the composition of the precipitate and resultant particle size.[1,4,9] Initial mixing of precursors is an extremely important variable in precipitation reactions. When large vessels are used, control of mixing is very difficult and tubular reactors are reported to solve some of the problems associated with batch processes.[1,4,9] Sonication has been reported in the synthesis of novel materials with unique properties.[1,6−8] Thus, the combination of selective heating and controllable liquid atomization could limit the drawbacks associated with batch coprecipitation. Both components of this system have previously been used separately to synthesize different materials, but the uniqueness of this process for making ultrafine metal oxides is the combination of these components in one process.[10]

Recently, we have developed a novel method that combines in situ mixing (I), ultrasonic nozzle treatment (N), and microwave heating (M) in a so-called INM process.[10] The technique has been demonstrated to be convenient for the preparation of multicomponent metal oxides and catalysts with interesting characteristics and remarkable activities.[10] Other nanosize oxides such as layered double hydroxides (LDHs), ahktenskite ϵ'-MnO_2, monodispersed silica nanoparticles coated with methylmethacrylate film, and zeolite A, among other oxide materials, have also been successfully produced. The properties of the products were

* To whom correspondence should be addressed. Phone: (860) 486-2797. Fax: (860) 486-2981. E-mail: steven.suib@uconn.edu.
[†] Department of Chemistry, University of Connecticut.
[‡] Department of Chemical, Materials and Bimolecular Engineering, University of Connecticut.
[§] Department of Chemical Engineering, University of Massachusetts.
[||] Department of Chemistry, University of Massachusetts.

10.1021/jp075647l CCC: $40.75
Published on Web 01/12/2008

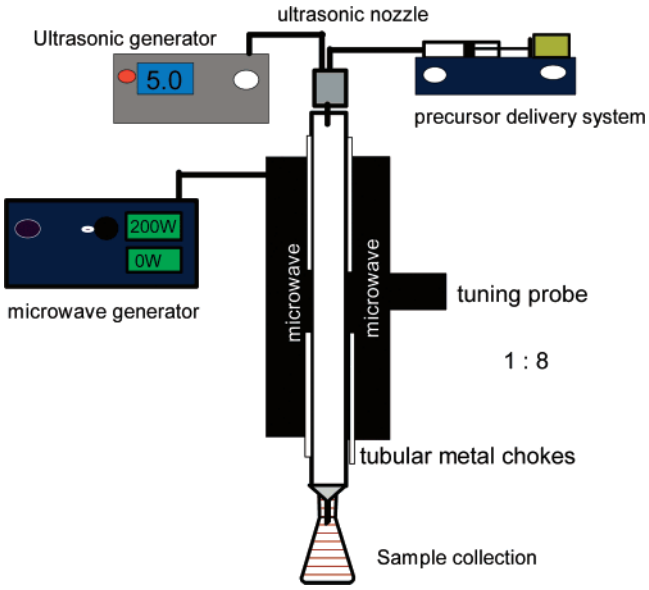

Figure 1. Schematic of continuous flow ultrasonic nozzle microwave (INM) reactor.

found to be dependent on the INM process rather than on subsequent treatments, i.e., calcination step.[10c]

Herein, we investigate the influence of microwave heating and ultrasonic nozzle mixing on the interfacial properties of the obtained materials. In the present work spinel metal oxides (nickel ferrites and zinc aluminates obtained by the coprecipitation technique in a conventional (without nozzle or microwave and conventional thermal heating) and in a continuous INM reactor were investigated. The synthesis of spinel metal oxides was investigated in order to study the effects of the nozzle and microwave treatment (INM process) on the composition, particle size, purity, and surface area of the resulting powders.

Experimental Section

Reactor Design. The INM continuous flow reactor design, Figure 1 consists of an ultrasonic nozzle (Sono-Tek Corp., Milton, NY, model Nos. 8700-48 and 8700-120 with a resonant frequency of 48 and 120 kHz,[11] respectively, Figure S1) that merges into one outlet of a vertical quartz or Teflon tube. The nozzle can be connected to 2 or more precursor aqueous solutions via an external syringe pump. Reactor tubes of diameter ranging from $\phi_o = 2.5-5.0$ cm and $l = 50.0-60.0$ cm are used. The microwave system used in this study was an internally tunable, cylindrical single-mode cavity operated at 2.45 GHz (Wavemat Microwave Processing System model CMPR 250, Plymouth, MI) with continuous power ranging from 0 to 1250 W. Tubular metal chokes ($\phi_i = 5.2$ cm; $\phi_o = 5.6$ cm) are employed to allow the reactor to pass through the cavity while impeding microwave emissions. After the precursor reaches the microwave cavity the product flowed continuously to a collection device. Conventional heating using a hot-walled furnace was also used instead of the microwave heating, Figure S2.

Synthesis. In a typical procedure, the metal cations are dissolved in distilled and deionized water. The molar ratio between the metal cations is calculated based on the desired product cation ratios. Nickel ferrite ($NiFe_2O_4$) and zinc aluminate ($ZnAl_2O_4$) were prepared by mixing their respective nitrate salts with distilled and deionized water in a ratio of 1:2. This solution was mixed and transferred to one 60-mL syringe. In a separate syringe, 60 mL of the precipitating reagent (0.6−1.2 M, NaOH or Na_2CO_3) was also prepared.

The syringe pump was used to regulate the flow rates of the starting materials and the precipitating agent, which were between 0.15 and 6.0 mL min^{-1}. The tubular reactor sits in a microwave chamber, and the resulting product was collected outside the cavity in a round-bottom flask. The material was dried at 80 °C overnight and calcined in air at 300−800 °C. Reference (control) syntheses for the INM method were also conducted. In the first control experiment, the synthesis was performed without nozzle or microwave radiation; unatomized droplet mixture goes through a tube at flow rate 1 mL/min. The second experiment was carried out with 120-kHz ultrasonic nozzle and without microwaves, while the third control experiment was conducted with 100−300-W microwave power and without nozzle in a noncontinuous mode (batch) for 5−10 min. Precursors of the same concentration as those used in INM were used. Conventional heating was also used instead of microwave heating and this process is referred to as INC for in situ (I), nozzle (N), conventional heating (C).

Characterization. Powder XRD data were collected on a Scintag PDS 2000 diffractometer utilizing a Cu Kα X-ray radiation with a voltage of 45 kV and current of 40 mA. The crystallite size was determined using Scherer's equation, using the (311) and (411) reflections. The instrumental line broadening was corrected using a LaB_6 standard. The size and morphology of the product particle were studied using field emission scanning electron microscopy (FESEM) on a Zeiss DSM 982 Gemini instrument with a Schottky emitter at an accelerating voltage of 2 kV and a beam current of 1 μA. The samples were suspended in water and dispersed on Au−Pd-coated silicon chips previously mounted onto stainless steel sample holders using two-sided carbon tape. The products were further characterized by transmission electron microscopy (TEM) with a JEOL 2010 Fas-TEM at an accelerating voltage of 200 kV with an energy dispersive X-ray analysis (EDS) system. The samples were prepared by dispersing the material in 2-propanol. A drop of the dispersion was placed onto a carbon-coated copper grid and allowed to dry. The chemical composition of the samples was determined by EDS. Thermogravimetric analysis (TGA) and temperature-programmed desorption with mass spectroscopic detection (TPD-MS) were employed to study the thermal stability of the samples. The TGA experiments were performed with a TA instrument Model 2950 in a N_2 atmosphere. The temperature was increased from 30 to 900 °C at a rate of 10 °C/min. TPD-MS data was obtained by heating about 30 mg of the sample in a tube furnace equipped with an MSS-RGA mass spectroscopy detector (MKS instrument). The samples were degassed in a 30 mL/min He flow overnight and then heated under a 30 mL/min He flow at a heating rate of 10 °C/min from 30 to 900 °C. Raman spectra were obtained using a Renishaw 2000 Ramascope with a 633 nm helium ion laser as the excitation source. Fourier transform infrared (FTIR) spectra were recorded on a Jasco FTIR 410 spectrometer at room temperature. The dark nickel ferrite powders were diluted with KBr at a ratio of 1:100 and then pressed into pellets. Brunauer−Emmett−Teller (BET) surface area of the materials was calculated from the N_2 adsorption isotherms on a Micromeritics ASAP 2010 surface analyzer.

Results

X-ray Powder Diffraction. Representative X-ray powder diffraction patterns of the obtained nickel ferrite from experimental conditions summarized in Table 1 are shown in Figure 2. The crystallite size was calculated using the Debye−Scherer formula.[12] The products obtained without the nozzle and

TABLE 1: Experimental Conditions of Nickel Ferrite and Results from XRD and Raman

sample	nozzle (kHz)	power (W/°C)	flow rate (mL min^{-1})	calcination temp (°C)	XRD crystallite size (nm)	phases present
1	no nozzle	no irradiation	1	800	39[a], 22[b]	$NiFe_2O_4$ + impurities
2	no nozzle	100	1	800	46[b]	$NiFe_2O_4$ + impurities
3	no nozzle	300	1	800	13[a]	$NiFe_2O_4$ + impurities
4	no nozzle	300	batch (10 min)	800	15[b]	$NiFe_2O_4$ + impurities
5	120	100	1	800	29[a], 18[b]	$NiFe_2O_4$ + impurities
6	120	no irradiation	1	800	7[a], 6[b]	$NiFe_2O_4$ + impurities
7	120[c]	300	1	800	15[b]	$NiFe_2O_4$ + impurities
8	120	300	1	600	6[b]	$NiFe_2O_4$
9	120	300	1	800	9[a], 13[b]	$NiFe_2O_4$
10	120	400	1	800	19[b]	$NiFe_2O_4$
11	120	300	3	800	19[a]	$NiFe_2O_4$ + impurities
12	no nozzle	no irradiation	1	600	not calculated	$NiFe_2O_4$ + impurities
13	120	100 °C	1	600	11	$NiFe_2O_4$
14	120	150 °C	1	600	10	$NiFe_2O_4$
15	48	300	1	600	8	$NiFe_2O_4$
16	120	300	1	600	12	$NiFe_2O_4$

[a] Refers to CO_3^{2-} as coprecipitating agent. [b] Refers to OH^- as coprecipitating agent. [c] Only co-ppt nozzle sprayed, cation solution inside the tube, $t = 10$ min.

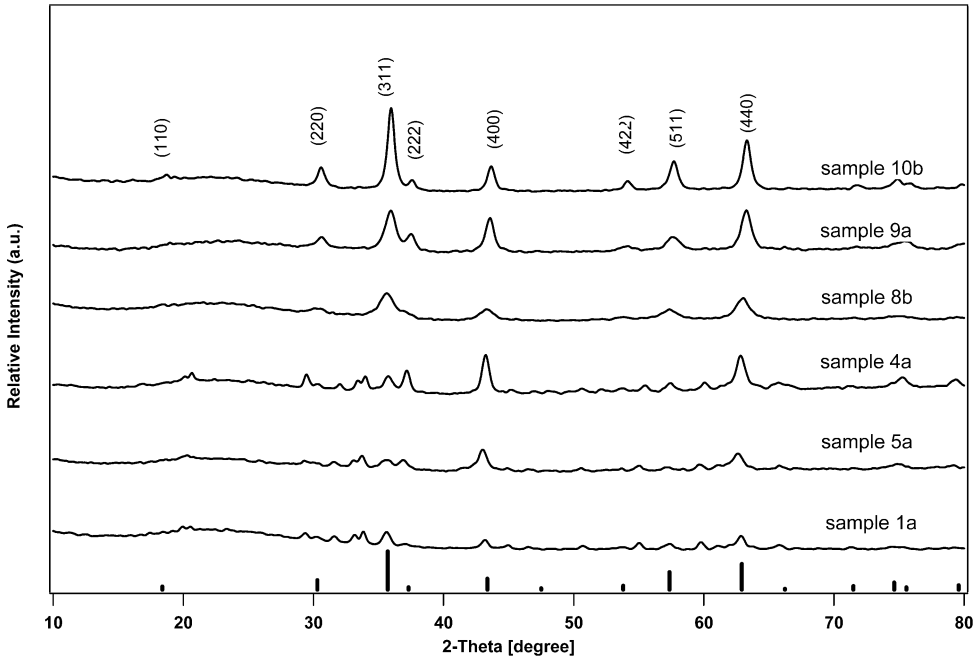

Figure 2. X-ray powder diffraction patterns of nickel ferrite (a) without microwave or ultrasonic nozzle mixing (sample 1a), (b) INM 100-W microwave 120-kHz nozzle (sample 5a), (c) 300 W without nozzle (batch) (sample 4a), (d) INM 300-W microwave with nozzle (sample 8b), (e) INM 300-W microwave with 120-kHz nozzle (sample 9a), (f) INM 400-W and 120-kHz nozzle (sample 10b). Vertical solid line, $NiFe_2O_4$ JCPDS No. 10-0325.

microwave irradiation have a cubic nickel ferrite spinel structure (JCPDS 10-0325) and also the following other phases: nickel oxide hydroxide (JCPDS 06-0044), hematite (JCPDS No. 33-0664), and goethite (JCPDS No. 17-0536), Figure 2a (sample 1). When the reagents were ultrasonically sprayed using the nozzle but without microwave irradiation, similar results were obtained (sample 6b). Use of 100-W microwave radiations and the ultrasonic nozzle resulted in secondary phases, as shown in Figure 2b (sample 5a). Control experiments without the ultrasonic nozzle but with starting materials being irradiated with microwaves at 300 W resulted in the formation of a spinel phase, along with other secondary phases, Figure 2c (sample 4b).

Materials produced via INM at 300−400 W and with 120-kHz ultrasonic nozzle show X-ray diffraction with corresponding *d* spacing of 2.94, 2.51, 2.09, 1.60, and 1.47 Å corresponding to the {220}, {311}, {400}, {511}, and {440} reflection of cubic nickel ferrite (2.95, 2.51, 2.09, 1.61, and 1.48 Å), respectively. The patterns correspond to only a *single-phase nanocrystalline product*, parts d and e of Figure 2 (samples 8b, 9a, and 10b). These trends were observed for the carbonate as well as hydroxide precipitation conditions, Table 1. The average crystallite size of different experiments varied from 6 to 46 nm.

Figure 3 shows powder X-ray diffraction (XRD) patterns of products prepared from optimized continuous flow conditions with either conventional or microwave heating (samples 12−16) followed by heat treatment at 600 °C for 6 h at ramp rate of 10 °C/min under N_2 atmosphere. All the patterns except sample 12 matched perfectly with the standard $NiFe_2O_4$, parts b−e of Figures 3. The XRD patterns of sample 12 exhibit the presence of NiO (JCPDS No. 22-1189) and α-Fe_2O_3 (JCPDS No. 33-0664 impurities, along with nickel ferrite, Figure 3a.

Figure 4 illustrates the XRD patterns of zinc aluminate ($ZnAl_2O_4$) prepared from conditions presented in Table 2. The XRD patterns were matched with the standard spinel $ZnAl_2O_4$ phase (JCPDS file No. 05-0669). Syntheses of zinc aluminate also depicted similar trends to those observed in the nickel ferrite INM synthesis. In the first experiment, the synthesis was performed without nozzle or microwave radiation, Figure 4a

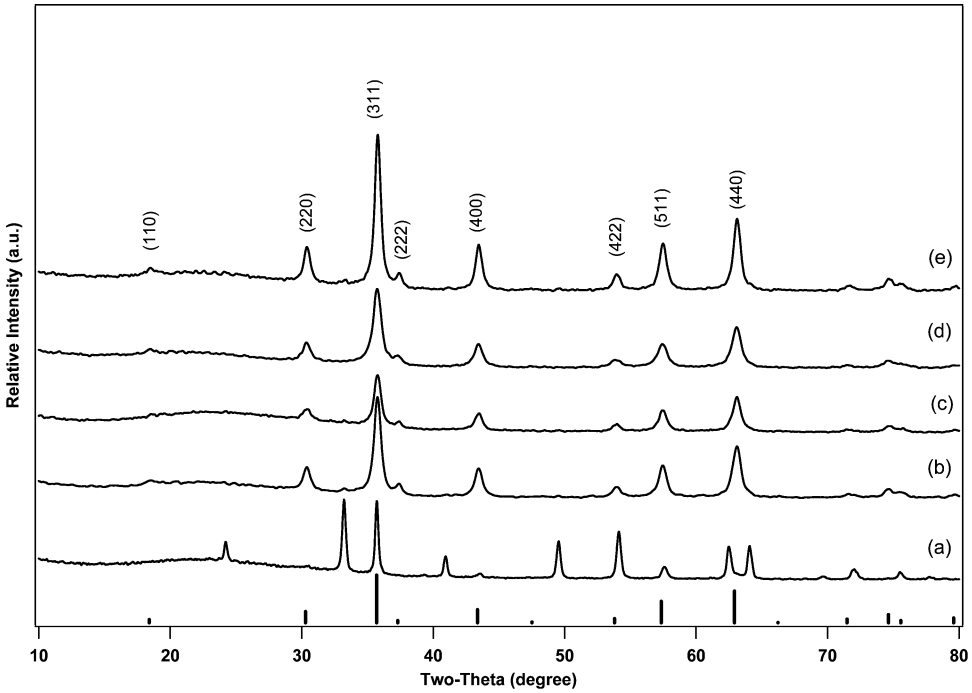

Figure 3. X-ray powder diffraction patterns of nickel ferrite. (a) Control experiment, no microwave nozzle, sample 12. (b) INC 120-kHz INC 100 °C, sample 13. (c) INC 120-kHz INC 150 °C, sample 14. (d) INM 48-kHz 300-W, sample 15. (e) INM 120-kHz 300-W, sample 16. Vertical solid line, $NiFe_2O_4$ JCPDS No. 10-0325.

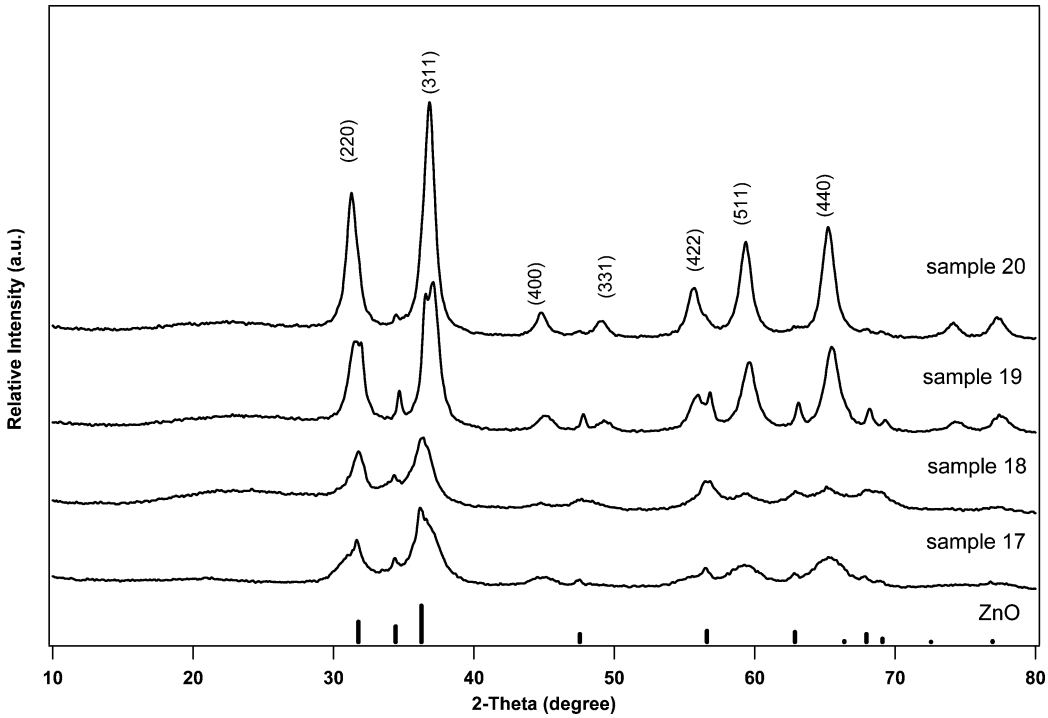

Figure 4. X-ray diffraction patterns of $ZnAl_2O_4$. (a) No microwave, no nozzle, sample 17; (b) no microwave 120 kHz, sample 19; (c) 300-W batch 5 min, sample 19; (d) INM 300-W 120-kHz nozzle, sample 20. Vertical solid line, hexagonal ZnO impurity peaks (JCPDS No. 36-1451).

TABLE 2: Experimental Conditions of Zinc Aluminate and Results from XRD

sample	nozzle (kHz)	power (W)	flow rate (mL min^{-1})	calcination temp (^oC)	XRD crystallite size (nm)	phases present
17	no nozzle	no irradiation	3	700	5	$ZnAl_2O_4 + ZnO$
18	120	no irradiation	3	700	6	$ZnAl_2O_4 + ZnO$
19	no nozzle	300	batch (5 min)	700	7	$ZnAl_2O_4 + ZnO$
20	120	300	3	700	9	$ZnAl_2O_4$

(sample 17). The second experiment was carried out with 120-kHz ultrasonic nozzle and without microwaves, Figure 4b (sample 18), while the third experiment was conducted with 300-W microwave power and no nozzle in a noncontinuous mode (batch) for 5 min, Figure 4c (sample 19). In all the experiments the product contained an impurity peak (ZnO,

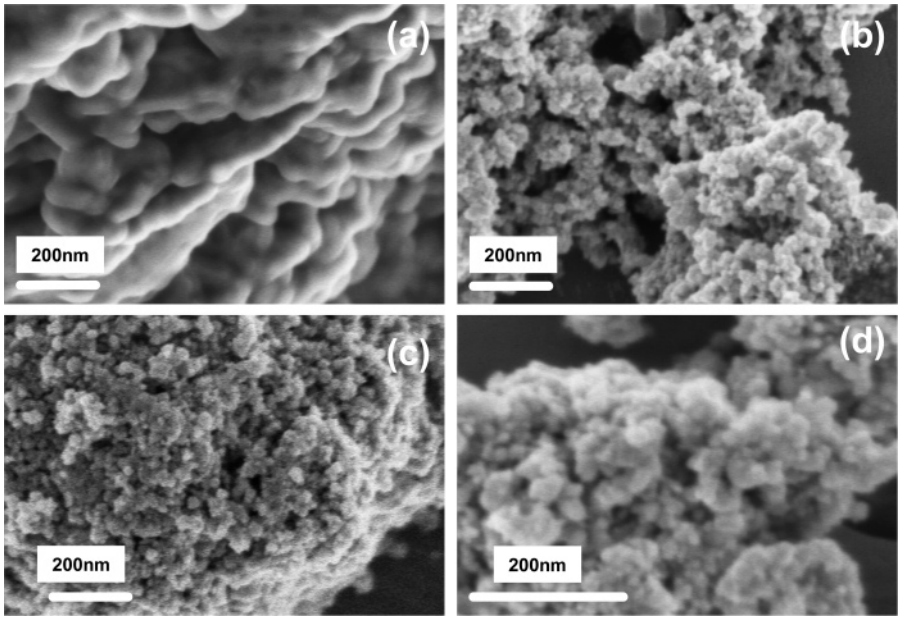

Figure 5. FESEM micrographs of (a) conventional mixing of nickel ferrite precursors (without nozzle or microwaves), sample 12. (b) INM 300-W microwave, 48-kHz nozzle, sample 15. (c) INM 300-W microwave, 120-kHz nozzle, sample 16. (d) INC 100 °C, 120-kHz nozzle, sample 13.

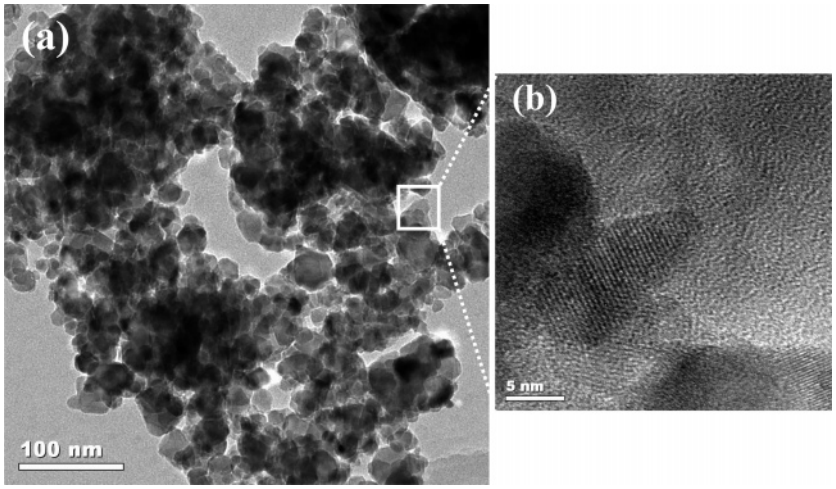

Figure 6. (a) Low- and (b) high-resolution TEM images of nickel ferrite nanocrystals, sample 16, prepared with the INM (300 W and 120-kHz nozzle) process.

JCPDS No. 36-1451). However, the fourth experiment INM 300 W, 120 kHz, Figure 4d (sample 20), resulted in predominantly *pure phase* zinc aluminate and small amounts of ZnO. Data of Table 2 show that the average crystallite size of different experiments varied from 5 to 9 nm. EDS measurements showed the presence of zinc and aluminum in the samples.

Microscopy. FESEM and TEM measurements were used to study the morphologies of the obtained products. Representative images of the products prepared from different conditions (with or without nozzle and microwaves/conventional) are shown in Figure 5. The micrographs show that the control product, sample 12 (without heating or ultrasonication: unatomized droplet mixture goes through a tube at flow rate 1 mL/min), exists as aggregated chunks, whereas the INM (300 W and 48 kHz nozzle) produced uniform slightly agglomerated spherical clusters, as shown in parts a and b of Figure 5, respectively. When 120-kHz nozzle is used the spherical clusters tend to agglomerate further, Figure 5c. Control experiments with conventional heating and 120-kHz nozzle show less uniform highly aggregated spherical particles, Figure 5d. Representative TEM and HR-TEM images (Figure 6) of sample 16 show that nanosize nickel ferrites are produced. The particles are roughly spherical and show lattice fringes that confirm the nanocystalline nature of nickel ferrite prepared by the INM process. EDS analysis revealed the existence of nickel, iron, and oxygen in these samples.

Vibrational Spectroscopy. FTIR was used to characterize the local environment of nickel and iron. Figure 7 shows the IR spectral studies of representative samples. These spectra illustrate absorption bands around 600 and 400 cm^{-1}, corresponding to the Fe−O and Ni−O bonds, respectively. These bands are typically associated with pure $NiFe_2O_4$.[13] The bands around 3500 cm^{-1} are assigned to the O−H stretching modes. The obtained products were further investigated using Raman spectroscopy, see Figure 8, in order to differentiate $NiFe_2O_4$ from other possible phases, such as γ-Fe_2O_3 and Fe_3O_4, which have a similar spinel structure and hence similar XRD patterns.[14,15] The FTIR spectroscopy confirmed that for the INM products the local environments of nickel and iron in the crystal structure are consistent with pure nickel ferrite, parts c−e of Figure 9. Raman peaks observed in parts a−c of Figure 8 for the optimized INM process can be assigned to a pure nickel

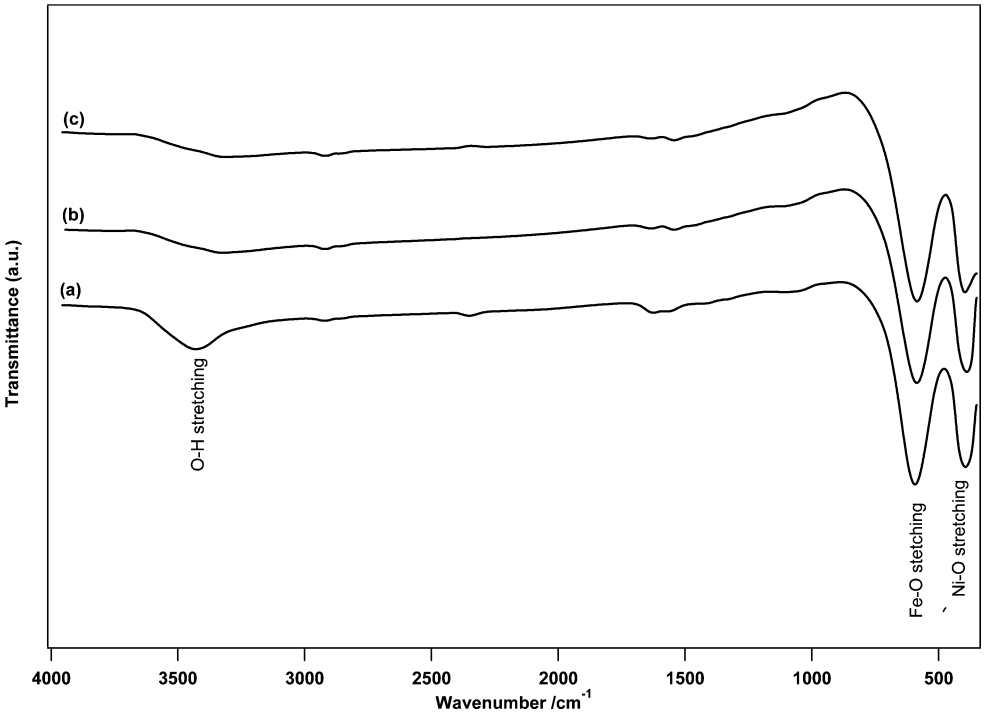

Figure 7. The FTIR spectra of nickel ferrites: (a) INM 300-W microwave, 48-kHz nozzle, sample 15; (b) INM 300-W microwave, 120-kHz nozzle, sample 16; (c) INC 100 °C, 120-kHz nozzle, sample 13.

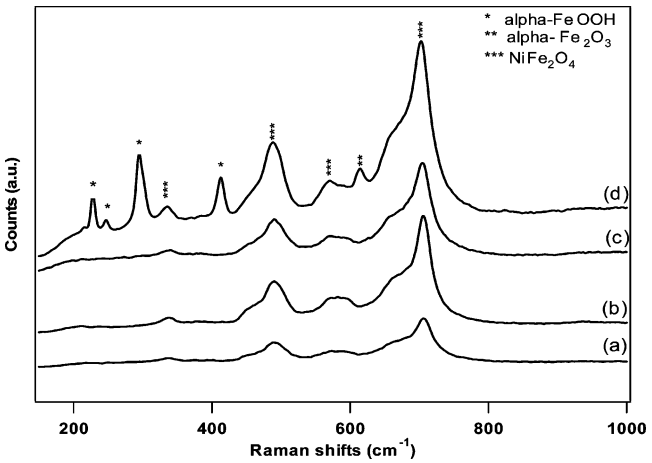

Figure 8. Raman spectra of (a) INM 300-W 120-kHz (OH^-), sample 9b; (b) INM 300-W 120-kHz (CO_3^{2-}), sample 9a; (c) INM 300-W 120-kHz, sample 8b; (d) no microwave, 120-kHz, sample 6b.

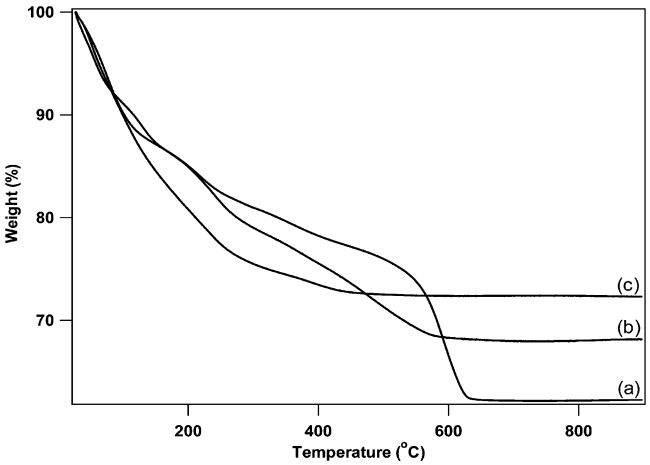

Figure 9. TGA curves of (a) without both microwave and ultrasonic nozzle treatment, sample 1b, (b) 300 W without nozzle, sample 4b, and (c) INM 300-W microwave and 120-kHz nozzle, sample 9b.

ferrite phase. However, control experiments without microwave irradiation but with a 120-kHz nozzle, Figure 8d, showed the existence of impurity phases in the composition. The impurities were matched to goethite (α-FeOOH) and hematite (α-Fe_2O_3).

Thermal Analysis. Representative TGA results are displayed in parts a−c of Figure 9. Nickel ferrite prepared at different conditions without nozzle and microwaves show a variation in the TGA curves. The TGA profile of the INM produced nickel ferrite sample, Figure 10c, exhibits two distinct weight loss steps in the temperature range 30−900 °C. The first weight loss step in the temperature range of 110−150 °C is attributed to desorption of physically adsorbed water on the surface of the products. The second step observed between 110 and 250 °C is ascribed to the decomposition of iron and nickel hydroxides. No weight losses were observed for this sample above 420 °C. The weight loss around 600 °C in sample 9a is attributed to simultaneous evolution of lattice oxygen and the decomposition nickel ferrite precursor. TPD-MS studies show that O_2 and NO gases are evolved at this temperature, Figure S3 of Supporting Information. The TGA of INM (300 W with 120-kHz nozzle) showed a total weight loss of 25 wt %, 32 wt % for the batch product (300 W without nozzle), and 40 wt % when no microwave or nozzle was used, parts a−c of Figure 9, respectively.

Surface Area. The BET surface areas of the prepared nickel ferrites, samples 13−16, are shown in Figure 10. The nickel ferrite spinels obtained from INM process (samples 13−14) have marginally higher surface areas than those obtained from the INC process (samples 15−16), 57−72 and 48−54 m^2/g, respectively.

Discussion

Effect of Ultrasonic Nozzle and Microwave Power on Phase Purity, Particle Size, and Surface Area of Nickel Ferrite and Zinc Aluminate. Initial mixing of the starting materials is critical in precipitation reactions. The nozzle has

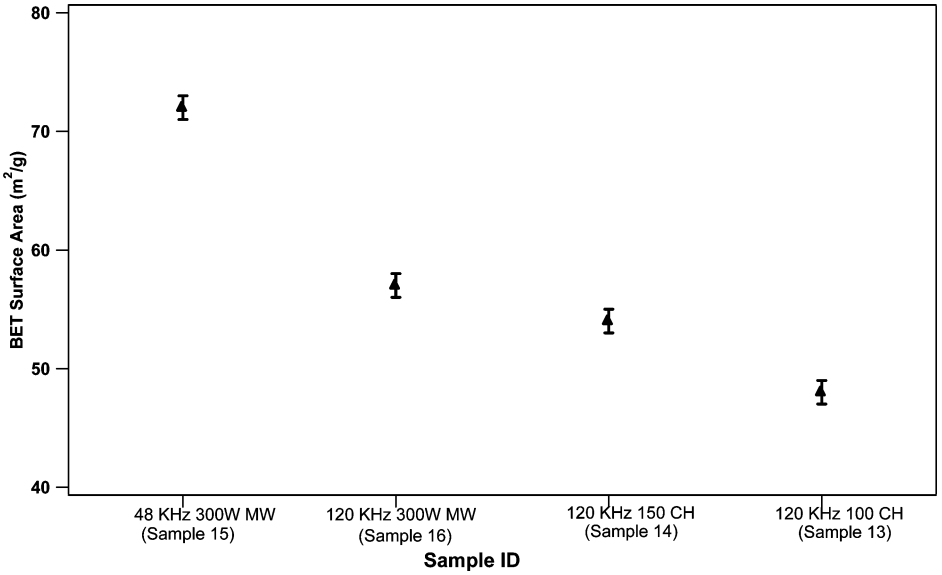

Figure 10. BET surface area of spinel nickel ferrites, samples 13−16.

an influence on the formation of the products. When no nozzle was used and the starting materials were simply flowed into the test tube, the product obtained after calcination was impure regardless of microwave power. The average crystallite size is between 15 and 46 nm (samples 1−2) and 6 nm (sample 17) for nickel ferrite and zinc aluminate, respectively. These data clearly show that nanosize particles are formed via INM methods. When the nozzle was used with microwave power of less than 300 W, no single-phase products were obtained (samples 5, 6, and 18). Control experiments performed without employing ultrasonic nozzle but with microwave irradiation at 300 W in batch and continuous modes also resulted in multiple phase products (samples 3, 4, and 19). Similar results of multiphase products were also obtained when only the precipitating agent was atomized using the nozzle, while the cation solution was irradiated with microwaves at 300 W (sample 7).

In contrast, when the microwave power setting of 300−400 W and 120-kHz nozzle were utilized, phase pure products were obtained (samples 8−10 and 20). For nickel ferrite, increasing the flow rate from 1 to 3 mL/min led to formation of an impurity phase (sample 10). The type of precipitation agent had no influence on the purity of the obtained products. However, the average crystallite size of the products was affected by microwave power, nozzle, annealing temperature, and type of the coprecipitation agent. In general, use of the nozzle and lower calcination temperatures resulted in smaller crystallites. No general trends could be deduced from microwave power and type of coprecipitation agent used. This could be due to unique interactions of the atomized reagents with microwaves.

The SEM of the control experiment, achieved by flowing the reactant mixture without ultrasonic nozzle mixing and microwave irradiation, resulted in large assemblages of large agglomerated particles, Figure 5a. XRD and Raman results indicated that products were impure and hence confirmed the earlier results that the high degree of mixing of precursors and microwave heating were responsible for the purity of the obtained particles and not a consequence of heat treatment of the precursor mixture. Parts b and c of Figure 5 revealed that the nozzle frequency (droplet size) affects the morphology of the resultant particles. High-frequency ultrasonic nozzle mixing (120 kHz) results in extended particle agglomeration, Figure 5c, greater than when the low-frequency nozzle (48 kHz) is used, Figure 5b. This could be due to formation of smaller particles at 120 kHz that tend to agglomerate. The median water droplet diameter of 120 and 48 kHz is 18 and 38 μm, respectively.[11] Particle size is affected by precursor drop size.[6a] TEM images confirmed that nanocystalline nickel ferrites were produced. The particle sizes of the prepared nickel ferrites ranged from 5 to 20 nm. No significant differences in TGA profiles were observed for phase pure nickel ferrite samples prepared from different conditions, samples 8−10 and 13−16. Differences were only observed for samples with different phases, which was consistent with the Raman and XRD data.

These results show that suitable combination of both microwave radiation and the ultrasonic nozzle are necessary to obtain single-phase products. The results clearly show in our INM (in situ mixing nozzle microwave) method that the two components do complement each other. That is, using the nozzle or microwave separately will not result in a pure material. However, using both the nozzle and microwaves at optimized flow rates results in single-phase products. The in situ ultrasonic nozzle facilitates the mixing of the starting materials, and subsequently the optimum microwave irradiation acts on a thorough blend of droplet mixtures that flow continuously to the collection vessel. Moreover, the ultrasonic nozzles have only 1/10 000 the kinetic energy of pressure sprays,[11] and hence the precursor droplets are suspended in the reactor where the interaction with the microwave irradiations could be enhanced. The suppression of the impurity phases could also be attributed to the creation of hot components by both the microwaves and the ultrasonic nozzle.[7a,16] Microwave heating could also promote diffusion and mixing[5d] of the reagents and thereby facilitate the complete conversion of the starting materials to single-phase products. In addition, microwave heating could be desirable for continuous processes due to high-energy transfer capabilities as volume to time ratio (flow rate) is significantly lower than the volume used in batch reactors.[5c] In addition, the highly controllable spray produced from in situ atomization produces reliable and consistent mixing of the precursor solutions. Further investigations of these systems in the synthesis of ultrafine metal oxides are ongoing.

Conclusions

The present study shows that nanocrystalline nickel ferrite with average crystallite size of 6−20 nm and surface areas

ranging from 57 to 72 m^2/g can be prepared from a new continuous method that combines microwave heating and ultrasonic nozzle mixing followed by thermal heat treatments. The INM method was also used to prepare zinc aluminate nanoparticles with an average crystallite size of about 9 nm. The use of low-frequency ultrasonic nozzle in situ mixing (48 kHz) with microwave heating resulted in marginally higher surface area of nickel ferrite nanoparticles than with 120-kHz nozzle.

Acknowledgment. We thank Mr. James Romanow for providing access to FESEM facilities in the Physiology and Neurobiology Department, University of Connecticut. We also acknowledge Dr. Francis S. Galasso for helpful discussions and support of the National Science Foundation NIRT Award No. CTS-0304217.

Supporting Information Available: Photos of the nozzle and the reactor and TPD-MS profiles. This material is available free of charge via the Internet at http://pubs.acs.org.

References and Notes

(1) (a) Cushing, B. L.; Kolesnichenko, V. L.; O'Connor, C. J. *Chem. Rev.* **2004**, 104, 3893. (b) Jongen, N.; Lamaitre, B. P.; Hoffmann, H. *Chem. Mater*. **1999**, *11*, 712. (c) Alvarez, G. S.; Mohammed, M.; Zagorodni, A. A. *Chem. Eng. Sci.* **2006**, *61*, 4625. (d) Letichevsky, Y.; Sominski, L.; Moreno, J. C.; Gadanken, A. *New J. Chem.* **2005**, *29*, 1445. (e) Kim, D. J.; Kroeger, D. M. *J. Mater. Sci.* **1993**, *28*, 4744. (f) Cote, L. J.; Teja, A. S.; Wilkinson, A. P.; Zhang, Z. J. *Fluid Phase Equilib.* **2003**, *210*, 307. (g) Liu, C.; Zou, B.; Rondinone, A. J.; Zhang, Z. J. *J. Phys. Chem. B* **2000**, *104*, 1141. (h) Hirai, T.; Kobayyashi, J.; Komasawa, I. *Langmuir* **1999**, *15*, 6291. (i) Moreno, E. M.; Zayat, M.; Morales, M. P.; Serna, C. J.; Roig, A.; Levy, D. *Langmuir* **2002**, *18*, 4972. (j) Jongen, N.: Donnet, M.; Bowen, P.; Lemaître, J.; Hofmann, H.; Schenk, R.; Hofmann, C.; Aoun-Habbache, M.; Guillemet-Fritsch, S.; Sarrias, J.; Rousset, A.; Viviani, M.; Buscaglia, M. T.; Buscaglia, V.; Nanni, P.; Testino, A.; Herguijuela, J. R. *Chem. Eng. Technol.* **2003**, *26*, 3, 303.

(2) (a) Oskam, G. *J. Sol−Gel Sci.* **2006**, *37*, 161. (b) Wang, X.; Zhang, J.; Peng, Q.; Li, Y. *Nature* **2005**, *437*, 121. (c) Dhage, S. R.; Khollam, Y. B.; Potdar, H. S.; Beshpande, S. B.; Bakare, P. P.; Sainker, S. R.; Date, S. K. *Mater. Lett.* **2002**, *57*, 457. (d) Voogt, F. C.; Fuji, T.; Smulders, P. J. M.; Nielsen, L.; James, M. A.; Hibma, T. *Phys. Rev. B* **1999**, *60*, 11193. (e) Nathani, H.; Gubbala, S.; Misra, R. D. K. *Mater. Sci. Eng. B* **2005**, *121*, 126. (f) Zhou, J.; Ma, J.; Sun, C.; Xie, L.; Zhao, Z.; Tian, H.; Yonggang, T.; Jiantao, Z.; Zhu, X. *J. Am. Ceram. Soc.* **2005**, *88*, 3535. (g) Leisle-Pelecky, D. L.; Rieke, R. D. *Chem. Mater*. **1996**, *8*, 1770. (h) Vestel, C. R.; Zhang, Z. J. *Int. J. Nanotechnol*. **2004**, *1*, 240. (i) Cannas, C.; Musinu, A.; Peddis, D.; Piccaluga, G. *J. Am. Chem. Soc.* **2006**, *18* (16), 3835. (j) Feng, L.; Junjie, L.; David, G. E.; Xue, D. *Chem. Mater.* **2004**, *16*, 1597. (k) Cesteros, Y.; Salagre, P.; Medina, F.; Sueiras, J. E. *Chem. Mater*. **2000**, *12*, 331.

(3) (a) Cabanas, A.; Darr, J. A.; Lester, E.; Poliakoff, M. *J. Mater. Chem.* **2001**, *11*, 561. (b) Adschiri, T.; Hakuta, Y.; Arai, K. *Ind. Eng. Chem. Res.* **2000**, *39*, 4901.

(4) Lin, X. Z.; Terepka, A. D.; Yang, H. *Nano. Letter* **2004**, *4* (11), 2227.

(5) Galema, S. A. *Chem. Soc. Rev.* **1997**, *26*, 233. (b) Tompsett, G. A.; Conner, W. C.; Yngvesson, K. S. *Chem. Phys. Chem.* **2006**, *7*, 296. (c) Clark, D. E.; Sutton, W. H. *Annu. Rev. Mater. Sci.* **1996**, *26*, 299. (d) Comer, E.; Organ, M. G. *J. Am. Chem. Soc.* **2005**, *127*, 8160. (e) Nissinen, T. A.; Kiros, Y.; Gasik, M.; Leskelä, M. *Chem. Mater*. **2003**, *15*, 4974. (f) Parada, C.; Moràn, E. *Chem. Mater*. **2006**, *18*, 2719. (g) Ying, J.; Wei-Wei, W.; Rui-Juan, Q.; Xian-Luo, H. *Angew. Chem., Int. Ed.* **2004**, *43*, 1410. (h) Adam, D. *Nature* **2003**, *421*, 571.

(6) (a) Tsai, S. C.; Song, Y. L.; Tsai, C. S.; Yang, C. C.; Chiu, W. Y.; Lin, H. M. *J. Mater. Sci.* **2004**, *39*, 3647. (b) Kerner, A.; Palchik, O.; Gedanken, A. *Chem. Mater*. **2001**, *13*, 1413. (c) Weixia, T.; Hanfan, L. *Chem. Mater.* **2000**, *12*, 564.

(7) (a) Suslick, K. S. *Science* **1990**, *247*, 1439. (b) Suslick, K. S.; Price, G. J. *Annu. Rev. Mater. Sci.* **1999**, *29*, 295. (c) Bang, J.-H.; Suslick, K. S. *J. Am. Chem. Soc.* **2007**, *129*, 2242.

(8) (a) Gedaken, A. *Ultrason. Sonochem.* **2004**, *11*, 47. (b) Okuyama, K.; Lenggoro, W. I. *Chem. Eng., Sci.* **2003**, *58*, 537. (c) Milošević, O. B.; Mirković, M. J.; Uskoković, D. P. *J. Am. Ceram. Soc*. **1996**, *79* (6), 1720.

(9) Tanaka, K.; Gomi, K.; Kamiya, H. *J. Ceram. Soc. Jpn.* **2003**, *111* (1), 67.

(10) (a) Suib, S. L.; Espinal, L.; Nyutu, E. K. U.S. Patent No. 20060291827, December 28, 2006. (b) Gaffney, A. M.; Espinal, L.; Le, D.; Suib, S. L. Eur. Patemt 06250531.8, April 2006. (c) Espinal, L.; Malinger, K.; Espinal, A.; Gaffney, A. M.; Suib, S. L. *Adv. Funct. Mater.* **2007**, 2572.

(11) Sono-Tek Corporation homepage: http://www.sono-tek.com/index.php (accessed October 20, 2007).

(12) (a) Klug, H.; Alexander, L. *X-ray Diffraction procedures*; Wiley: New York, 1962; p 125. (b) Cullity, B. D.; Stock, S. R. *Elements of X-Ray Diffraction*; Prentice Hall: New Jersey, 2001; p 170.

(13) Zhou, Z. H.; Xue, J. M.; Wang. J.; Chan, H. S. O.; Yu, T.; Shen, Z. X. *J. Appl. Phys.* **2002**, *91* (3), 6015.

(14) (a) Sousa, M. H.; Tourinho, F. A.; Rubim, J. C. *J. Raman Spectrosc.* **2000**, *31*, 185. (b) Bersani, D.; Loticci, P. P.; Montenero, A. *J. Raman Spectrosc.* **1999**, *30*, 355.

(15) Daou, T. J.; Pourroy, G.; Bégin-Colin, S.; Greneche, J. M.; Ulhaq-Bouillet, C.; Legaré, P.; Bernhardt, P.; Leuvrey, C.; Rogez, G. *Chem. Mater.* **2006**, *18*, 4399.

(16) Blanco, C.; Auerbach, S. M. *J. Am. Chem. Soc.* **2002**, *124*, 6250.